Atmospheric Research 155 (2015) 1–12

Contents lists available at ScienceDirect

Atmospheric Research

journal homepage: www.elsevier.com/locate/atmos

Optical properties of size-resolved particles at a Hong Kong urban site during winter

Yuan Gao [a], Senchao Lai [b], Shun-Cheng Lee [a,*], Pui Shan Yau [a], Yu Huang [a,d], Yan Cheng [c], Tao Wang [a], Zheng Xu [a], Chao Yuan [a], Yingyi Zhang [b]

[a] Department of Civil and Environmental Engineering, Research Center for Environmental Technology and Management, The Hong Kong Polytechnic University, HungHom, Kowloon, Hong Kong
[b] College of Environment and Energy, South China University of Technology, Higher Education Mega Centre, Guangzhou 510006, China
[c] Department of Environmental Science and Technology, School of Human Settlements and Civil Engineering, Xi'an Jiaotong University, No. 28 Xianning West Road, Xi'an, Shaanxi, 710049, China
[d] Key Lab of Aerosol Chemistry and Physics, Institute of Earth Environment, Chinese Academy of Sciences, Xi'an, 710075, China

ARTICLE INFO

Article history:
Received 25 June 2014
Received in revised form 22 October 2014
Accepted 24 October 2014
Available online 1 November 2014

Keywords:
Size-resolved PM
Aerosol light extinction
Chemical species
Source apportionment

ABSTRACT

Visibility degradation in Hong Kong is related to the city's serious air pollution problems. To investigate the aerosols' optical properties and their relationship with the chemical composition and size distribution of the particles, a monitoring campaign was conducted at an urban site in the early winter period (from October to December, 2010). The particle light scattering coefficient (B_{sp}) and absorption coefficient (B_{ap}) were measured. Two collocated Micro-Orifice Uniform Deposit Impactor samplers (MOUDI110, MSP, USA) with nominal 50% cut-off aerodynamic diameters of 18, 10, 5.6, 3.2, 1.8, 1, 0.56, 0.32, 0.18, 0.1, and 0.056 μm were used to collect size-resolved particle samples. The average B_{sp} and B_{ap} were 201.96 ± 105.82 Mm^{-1} and 39.91 ± 19.16 Mm^{-1}, with an average single scattering albedo (ω_o) of 0.82 ± 0.07. The theoretical method of light extinction calculation was used to determine the extinction of the size-resolved particulate matters (PM). The reconstructed light scattering coefficient correlated well with the measured scattering value in the Hong Kong urban area. Droplet mode (0.56–1.8 μm) particles contributed most to the particle light extinction (~69%). Organic matter, ammonium sulphate and elemental carbon were the key components causing visibility degradation in the droplet (0.56–1.8 μm) and condensation (0.1–0.56 μm) size ranges. Five sources contributing to particle light extinction have been identified using positive matrix factorisation (PMF). Traffic/engine exhausts and secondary aerosols accounted for ~36% and ~32% of particle light extinction, respectively, followed by sea salt (15%). The remaining sources, soil/fugitive dust and tire dust, contributed by ~10% and 7%, respectively, to particle light extinction.

1. Introduction

Visibility impairment results from the scattering and absorption of incoming sunlight (Tao et al., 2009; Watson, 2002). The light extinction (B_{ext}) can be used to describe its characteristics, providing a summation of light scattering and absorption from particulate and gaseous matter (Bohren and Huffman, 2008). Natural and pollution-derived particles disturb the Earth's radiation balance and indirectly affect cloud formation and climate change (Bohren and Huffman, 2008; Ling et al., 2013; Rosenfeld, 1999; Yan et al., 2008). Particle optical properties are highly related to particle sizes, shapes and chemical components (Tsai et al., 2012; Yan et al., 2008; Yu et al., 2010).

* Corresponding author. Tel.: +852 27666011; fax: +852 23346389.
E-mail address: ceslee@polyu.edu.hk (S.-C. Lee).

http://dx.doi.org/10.1016/j.atmosres.2014.10.020
0169-8095/

The frequency of low visibility days in Hong Kong has increased over the last decade (HKO, 2013). Past studies (Chang and Koo, 1986; Cheung et al., 2005; Lai and Sequeira, 2001; Lee and Sequeira, 2002; Man and Shih, 2001; Sequeira and Lai, 1998; Wang et al., 2003) have shown that ammonium sulphate ($(NH_4)_2SO_4$) and elemental carbon (EC) are the most important factors causing this visibility impairment. Ammonium sulphate is a hydrophilic compound, and its resulting increase in relative humidity (RH) can enhance its light scattering effect. Many methods have been used to determine the scattering and absorption efficiency of chemical components, including the theoretical method, the partial scattering method, the measurement method and the multilinear regression (MLR) method (Hand and Malm, 2007). The theoretical and partial scattering methods have been used to determine the scattering and absorption efficiencies of chemical components in the USA. (Lowenthal and Kumar, 2004, 2006; Malm and Pitchford, 1997; Sloane, 1986). In Hong Kong, the MLR method and the US Interagency Monitoring of Protected Visual Environments (IMPROVE) equation have commonly been used to determine the contributions of different chemical components to visibility impairment in $PM_{2.5}$ and PM_{10} (Wang et al., 2003). A small number of studies have focused on determining the optical properties of size-resolved particles (Lowenthal et al. 1995; Sloane and Wolff, 1985).

In this study, optical parameters were measured and size-fractionated chemical components (i.e., elements, water soluble ions and carbon) were analysed hourly during the winter period at an urban site in Hong Kong. The study aims to 1) determine the characteristics and variations of the optical properties of size-segregated particles in an urban environment; 2) provide insight into size-resolved particles and their chemical extinction (the summation of (mass concentration × their mass extinction efficiency) for different chemical components) by using the theoretical method; and 3) identify potential sources contributing to particle light extinction.

2. Methods

2.1. Sampling site

Hong Kong occupies an area of 1104 square kilometres, with a population of seven million; it is one of the developed cities in the world (World Bank, 2011). The sampling site was located on the rooftop of an eight-floor building on the campus of the Hong Kong Polytechnic University (HKPU) (22.30°N, 114.17°E), as shown in Fig. 1. This site is close to the Cross Harbour Tunnel, subject to heavy traffic activity and regional pollutant transport.

2.2. Continuous optical, gaseous and meteorological parameter measurements

The particle light scattering coefficients (B_{sp}) for fine suspended particles were measured hourly using an integrating nephelometer (wavelength, $\lambda = 525$ nm) with a heater (Aurora-1000 Ecotech, Melbourne, Australia) to maintain the RH of <60%. The heated nephelometer may have caused some evaporation of ammonium nitrate, (NH_4NO_3), which is one of chemical components leading to visibility impairment (Watson et al., 2008b). To restrict the nephelometer uncertainty to within ±10%, its sampling tube was designed based on Bergin et al. (1997). Calibration was performed by a daily zero check (to within ±1 Mm^{-1}) and a monthly span check (not more than 10% of the recommended value). The zero check was performed automatically by pumping in particle-free air. The span check was performed manually using carbon dioxide (CO_2), as recommended by the manufacturer (Aurora-1000 User Manual, 2008). Hourly black carbon (BC) concentrations ($\mu g/m^3$) were measured using an aethalometer with a flow rate of 5 L/min (Magee Scientific Company, Berkeley, CA, USA, Model AE-31). The particles absorption coefficient (B_{ap}) (Mm^{-1}) at $\lambda = 532$ nm was calculated from the BC

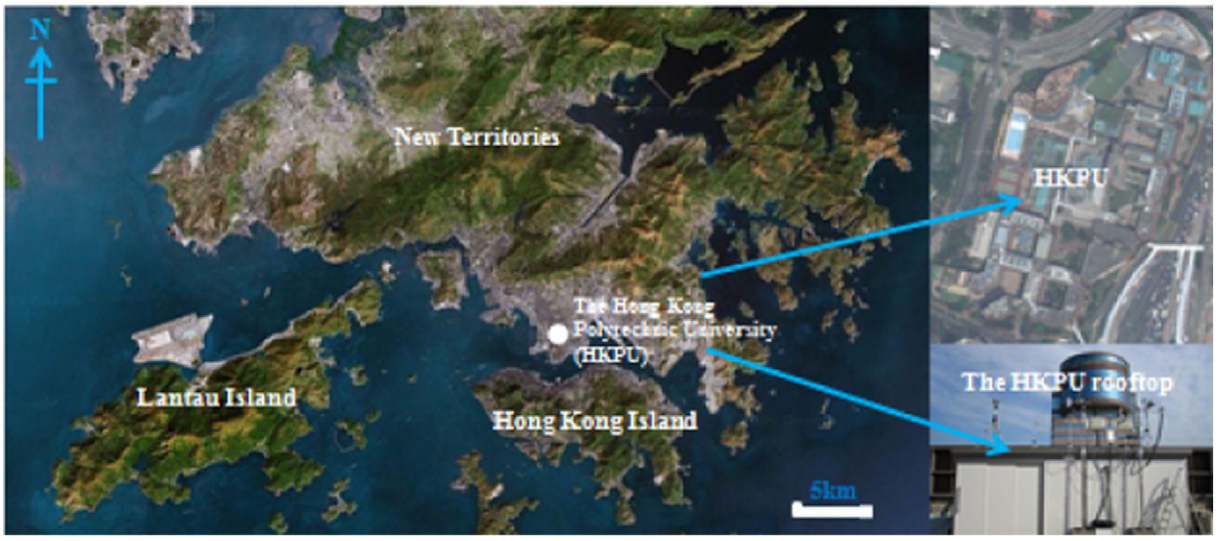

Fig. 1. Location of the sampling site, at the Hong Kong Polytechnic University, Kowloon.

concentration in μg/m^3 (λ = 880 nm), based on a mass absorption efficiency value of 8.28 m^2/g, using the equation $B_{ap\ (532\ nm)} = 8.28 \times [BC, \mu g/m^3]$ (Weingartner et al., 2003; Wu et al., 2009). To maintain the same wavelength (λ = 532 nm) between B_{sp} and B_{ap}, the hourly B_{sp} at 525 nm was converted by applying an Angström exponent (α_s) of 1.3 in the Pearl River Delta (PRD) region (Jung et al., 2009; Xu et al., 2012) based on the following equation, as described in Ångström (1930) and Rocard and de Rothschild (1927):

$$B_{sp}(532\ nm) = B_{sp}(525\ nm) \times \left(\frac{532\ nm}{525\ nm}\right)^{-\alpha_s} \quad (1)$$

The single scattering albedo (SSA, ω_o at λ = 532 nm) is an important factor in estimating radiative forcing (Yan et al., 2008). It was calculated based on the ratio of B_{sp} to the sum of B_{sp} and B_{ap} at 532 nm.

The hourly-averaged concentrations of inorganic water-soluble ions—chloride (Cl^-), nitrate (NO_3^-), sulphate (SO_4^{2-}), sodium (Na^+), ammonium (NH_4^+), potassium (K^+), calcium (Ca^{2+}) and magnesium (Mg^{2+})—were determined by Ambient ions monitoring (AIM) using a Dionex IC Model 90 (Sunnyvale, California, USA). The process for the measurement of ion species by AIM is described in the studies of Zhou et al. (2009, 2012). Hourly nitrogen dioxide (NO_2) was measured using a chemiluminescence instrument (Model 42I Thermo Environmental instrument, Waltham, Massachusetts, USA; Xu et al., 2013). Concurrent meteorological parameters, such as wind direction (WD), wind speed (WS), relative humidity (RH), ambient temperature (T), and solar radiation, were measured using a portable automatic meteorological station (Model 05305VM and Model 41382 VC/VF, R.M. Young Company, Traverse City, Michigan, USA). Hourly gaseous, ionic, optical and meteorological measurements were taken from October 23, 2010 to December 31, 2010.

2.3. Integrated sample collection

Two collocated Micro-Orifice Uniform Deposit Impactor (MOUDI 100, MSP Corp., Shoreview, Minnesota, USA) samplers were operated at a 30 L/min flow rate. The MOUDI samplers had 10 stages with nominal 50% cut-offs at aerodynamic diameters of 18, 10, 5.6, 3.2, 1.8, 1, 0.56, 0.32, 0.18, 0.1, and 0.056 μm. A total of 10 sets of 24-h samples (including one field blank to assess passive deposition), were collected in 2010, each from 10:00 am of one day to 10:00 am of the next (LST, Local standard time; samples taken October 23rd, November 1st, 4th, 7th, 13th, 25th, December 1st, 5th and 11th) using Teflon-membrane (Φ = 47 mm, Pall Sciences, New York, USA) and quartz-fibre (47 mm QMA, Whatman, Maidtone, England) filters. The backup stage of the impactor used 37 mm Teflon-membrane and quartz-fibre filters.

Before sampling, the quartz-fibre filters were preheated at 900 °C for 3 h to minimise organic artifacts (Ho et al., 2006). Both the Teflon-membrane and quartz-fibre filters were weighed before and after sampling using a microbalance (Model MC5, Satorius, Goettingen, Germany) with a sensitivity of ±1 μg in the 0–250 mg range. Before weighing, the filters were equilibrated in a desiccator (DRY-100, WEIFO, TAIWAN) for 24 h in a temperature (25 ± 5 °C) and RH (35 ± 10%) controlled environment. After weighing, the filters were stored in air-tight containers in a refrigerator at 4 °C to prevent the evaporation of volatile components. Sample flow rates within ±10% of the specification were verified at the beginning and end of each sampling period.

Some uncertainty in the MOUDI sampler measurements resulted from the effects of temperature, relative humidity and particle bounce (Chow et al., 2005; Huang et al., 2004; Milford and Davidson, 1987). To eliminate these uncertainties, artifacts in the size-resolved particle concentration data were corrected using the method provided by Wang et al. (2013b); Nie et al. (2010). The MOUDI samples were categorised into two to three groups based on the degree of sampling loss. An averaged integrated loss degree, which was later used to constrain sampling losses, was estimated from a regression analysis between MOUDI and AIM for each group of samples determined earlier. The value resulting from subtraction of the MOUDI samples with and without sampling losses was used to derive a loss function for each size bin below a certain degree of integrated loss. The constrained loss percentages in each individual size range were used to correct the size-resolved MOUDI data.

2.4. Chemical analysis

After gravimetric analysis, Teflon-membrane filters were analysed for the presence of 51 elements (from Na to U) at the Institute of Earth and Environment, Chinese Academy of Science, China, using energy-dispersive X-ray fluorescence (XRF) analyses (Epsilon 5 ED-XRF, PANalytical B.V., the Netherlands; Watson et al., 1999). The quartz-fibre filters were analysed for organic carbon (OC), elemental carbon (EC) and water-soluble ions in the Air Laboratory of HKPU. A portion of the quartz-fibre filter samples (0.526 cm^2) were used for OC and EC analysis by the DRI Model 2001 Thermal/Optical Carbon Analyser (Atmoslytic Inc., Calabasas, CA, USA), following the IMPROVE-A/Thermal-Optical reference (TOR; Chow et al., 2007, 2011; Ho et al., 2002). For ion analysis, half of quartz-fibre filters were extracted with 10 ml of ultra-pure water (specific resistance ≥18.1 MΩ, Millipore). The extraction solutions were filtered and stored in plastic vials in the refrigerator at 4 °C until analysis. Water soluble ions including Cl^-, NO_3^-, SO_4^{2-}, Na^+, K^+, Ca^{2+} and NH_4^+ were analysed using ion chromatography (ICS3000, DIONEX, Sunnyvale, CA, USA; Chow and Watson, 1999).

Teflon-membrane filters were used to determine measured mass concentrations for different particle sizes. The reconstructed mass was calculated based on the mass reconstruction of the soil dust ($2.2 \times Al + 2.49 \times Si + 1.63 \times Ca + 2.42 \times Fe + 1.94 \times Ti$), organic matters ($OC \times 1.8$), soot (EC), ammonium sulphate ($1.375 \times SO_4^{2-}$), ammonium nitrate ($1.29 \times NO_3^-$) and non-crustal trace elements (the sum of non-geological trace elements). A reasonable correlation of R^2 = 0.90 was found between the measured and reconstructed mass concentrations. This result confirmed the validity of the gravimetric and chemical measurements. Supplemental Figures S1–S3 provide more detailed information on the validity of the chemical measurements, including reconstructed and measured mass, anion vs. cation balance, and internal consistency (i.e., sulphate vs. sulphur, chloride vs. chlorine).

Table 1
Densities and refractive indices of individual chemical components.

Component	Density (g/cm^3)	Refractive index	Reference
Ammonium sulfate $(NH_4)_2SO_4$	1.76	1.53, i0.0	(Watson et al., 2008b)
Ammonium nitrate $(NH_4)NO_3$	1.73	1.55, i0.0	(Watson et al., 2008b)
Organic matters (OM)	1.2	1.55, i0.0	(Watson et al., 2008b)
Elemental carbon (EC)	1.7	1.9, i0.6	(Watson et al., 2008b)
Soil	2.3	1.56, i0.005	(Watson et al., 2008b)
Sea salt	2.17	1.54, i0.0	(Tang, 1996)
Water content	1.00	1.33, i0.0	(Watson et al., 2008b)

2.5. Estimation of particle light scattering and absorption

The size-resolved particle scattering and absorption coefficient was calculated using Mie theory (Mie, 1908; Sloane, 1983, 1984, 1986; Sloane and Wolff, 1985):

$$B_{sp} = \int \sigma_{sp} n(D) dD, \tag{2}$$

where σ_{sp} is the scattering cross section, which depends on the incident light wavelength (λ), the stokes diameter (D; Cheng et al., 2008), and the complex index of refraction (m), which can be calculated using Mie theory for spherical particles (Bohren and Huffman, 2008; Rosenberg et al., 2012; Wiscombe, 1980). D is the particle diameter and $n(D)\ dD$ is the number concentration over the diameter interval dD. The MOUDI stage concentrations were converted to continuous size distributions using a log-normal distribution (Dong et al., 2004; Twomey, 1975; Winklmayr et al., 1990). The number concentration $n(D)dD$ was then determined from the mass concentrations of the different species (Sloane, 1984), using the following equation:

$$n(D)\ dD = \frac{M(D)}{\frac{\rho \times \left(\frac{D_a}{D}\right)^3 \times \pi \times D^3}{6}} \tag{3}$$

The ELSIE program is configured for five chemical components (USA IMPROVE; Sisler et al., 1996): soil dust (Eq. (5)), organic matter (Eq. (6)), ammonium sulphate (Eq. (7)), ammonium nitrate (Eq. (8)), and sea salt (Eq. (9)). Water content was estimated using the ZSR (Zdanovski–Stokes–Robinson) method (Clegg et al., 1998; Clegg and Seinfeld, 2004; Stokes and Robinson, 1966). The densities (ρ) and complex indices of refraction (m) obtained are shown in Table 1.

The particle light extinction (B_{ext}) was calculated as a summation of particle light scattering (B_{sp}) and particle light absorption (B_{ap}):

$$B_{ext} = B_{sp} + B_{ap} = \int \sigma_{sp} n(D) dD + \int \sigma_{ap} n(D) dD \tag{4}$$

where only the followed chemical species were considered and each species or element was multiplied by a molar correction factor (mcf), as in Malm et al. (1994):

$$\text{Soil dust} = 2.2 \times \text{Al} + 2.49 \times \text{Si} + 1.63 \times \text{Ca} + 2.42 \times \text{Fe} + 1.94 \times \text{Ti} \tag{5}$$

$$\text{Organic matters} = \text{OC} \times 1.8 \tag{6}$$

$$\text{Ammonium nitrate} = 1.29 \times NO_3^- \tag{7}$$

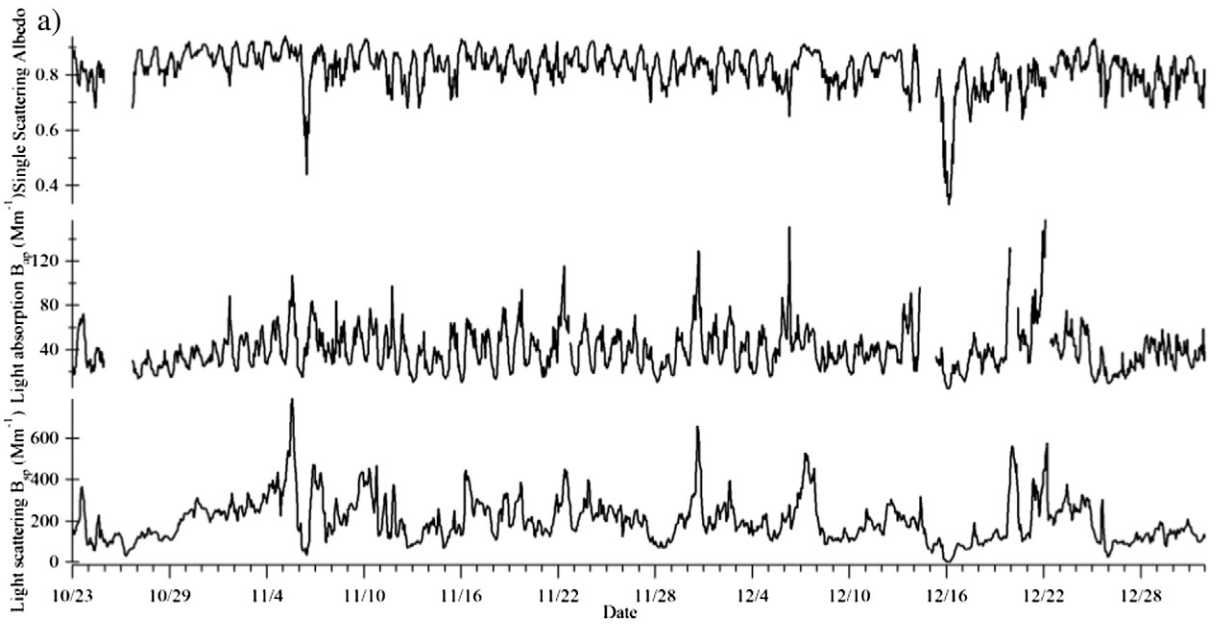

Fig. 2. a. Time series on hourly particle scattering coefficient (B_{sp}), absorption coefficient (B_{ap}) and single scattering albedo (ω_o). b. Frequency distribution of hourly particle scattering coefficient (B_{sp}), absorption coefficient (B_{ap}) and single scattering albedo (ω_o).

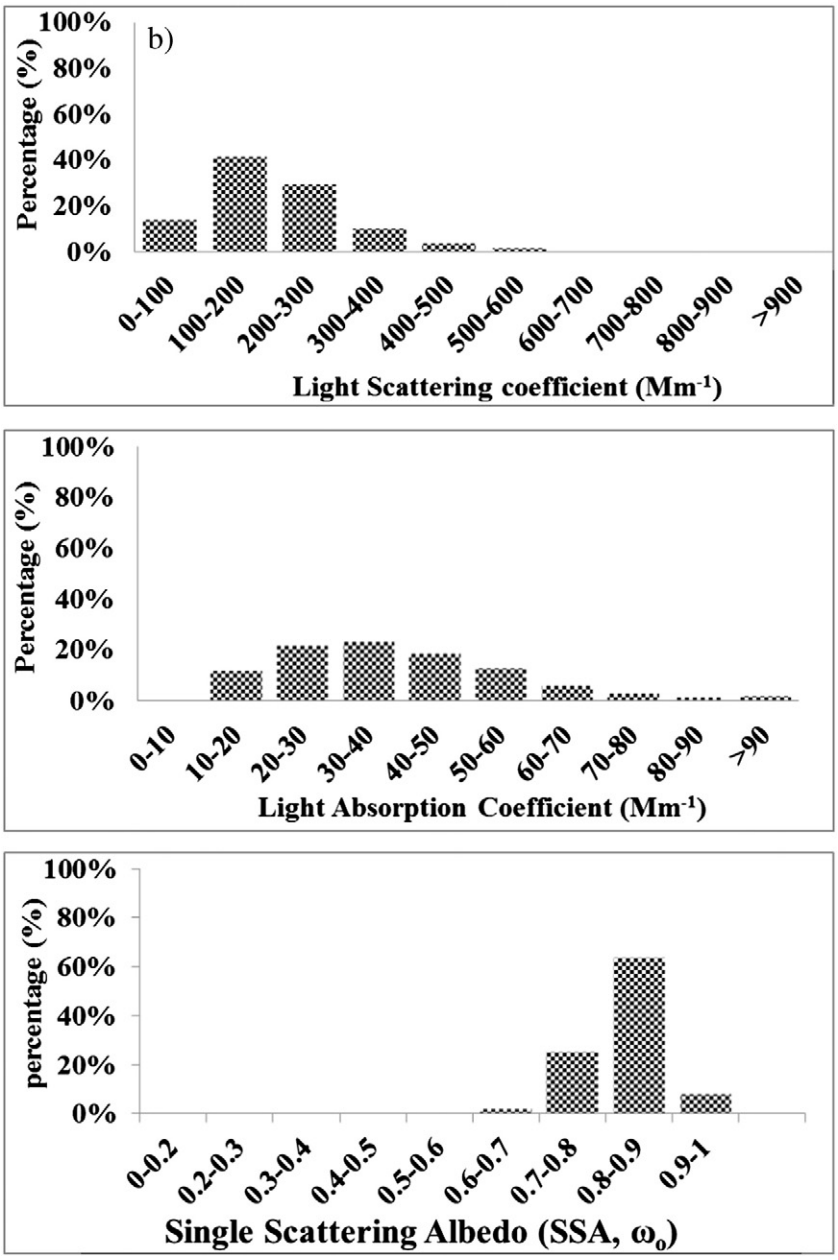

Fig. 2 (*continued.*)

$$\text{Ammonium sulphate} = 1.375 \times SO_4^{2-} \quad (8)$$

$$\text{Sea salt} = 1.8 \times Cl^- \quad (9)$$

It should be noted that only fine nitrate particles were considered as ammonium nitrate in the equation. The reasons for not considering coarse nitrate particles were 1) that coarse particles are not important for particle light extinction (Jung et al., 2009; Li et al., 2013); and 2) that the mass concentration of coarse nitrate particles in the study was less than 10% of the mass concentration of coarse particles.

In the study, particle light absorption was estimated using the following equations: $B_{ap} = \int \sigma_{ap} n(D) dD$ and $n(D)dD = \frac{M(D)}{\frac{\rho \times \left(\frac{D_0}{D}\right)^3 \times \pi \times D^3}{6}}$. The EC concentration was used to calculate particle light absorption. The density and refractive index of EC are given in Table 1.

2.6. Source apportionment of visibility degradation

The PMF model is a multivariate factor analysis method that functions by dividing speciated data into two matrices: factor contribution (g) and factor profile (f). It can be illustrated by the

Table 2
Summary of optical properties from 23 October to 31 December 2010.

Sampling site	Particle light scattering (B_{sp} at 532 nm)	Particle light absorption (B_{ap} at 532 nm)	Single scattering albedo (SSA, ω_o)[a]
The HK Polytechnic University (PU)	(Mm^{-1})	(Mm^{-1})	
Average	201.96	39.91	0.82
Standard deviation (SD)	105.82	19.16	0.07
Maximum	788.91	156.95	0.94
Minimum	2.43	4.77	0.33
Median	183.04	36.99	0.83
Hours	1679	1600	1600

[a] $\omega_o = \frac{B_{sp}}{B_{sp}+B_{ap}}$.

equation $X_{ij} = \sum_{k=1}^{p} g_{ik} f_{kj} + e_{ij}$, where i and j represent the number of samples (i) and chemical species (j); X_{ij} is a matrix in the i and j dimensions, and is related to the number of factors (p), the species profile (f) and the amount of mass for each factor (g). The method has been described and reviewed in detail by Paatero and Tapper (1994) and Paatero (1997). The model has previously been used to identify the potential sources for visibility degradation (Han et al., 2006; Watson et al., 2008a). The PMF model was run multiple times to extract five factors, and linear regression analysis similar to that used by Cao et al. (2012) was used to estimate the contribution of each source to light extinction.

3. Results and discussion

3.1. Aerosol optical property

Fig. 2a presents the hourly time series of B_{sp}, B_{ap} and Single Scattering Albedo (SSA, ω_o). Large variations were found in the hourly optical measurements, which ranged from 2.4 to 789 Mm^{-1} for B_{sp}, from 4.8 to 157 Mm^{-1} for B_{ap} and from 0.33 to 0.94 for ω_o (Table 2). The monthly B_{sp} and B_{ap} frequently reached 100–200 Mm^{-1} and 20–40 Mm^{-1}, respectively. Scattering accounted for a majority of particle light extinction; ω_o was mostly in the range of 0.8–0.9 (Fig. 2b).

In general, average B_{sp} and B_{ap} values in this study were 45–100% lower than those measured in Chinese mega cities such as Guangzhou, Shanghai and Beijing during the winter period (Andreae et al., 2008; He et al., 2009; Xu et al., 2012). However, the average B_{sp} (202 ± 106 Mm^{-1}) was ~50% to 70% higher than the values of 60 Mm^{-1}, 84 Mm^{-1} and 93 Mm^{-1}, measured at Valencia (Spain), Granada (Spain), and Southern Mexico city (Mexico), respectively, while the average B_{ap} of 40 ± 19 Mm^{-1} was ~30% to 40% higher (Garcia et al., 2010; Lyamani et al., 2008; Titos et al., 2012; Xu et al., 2012). The mean and median ω_o of 0.83 and 0.82 were similar to the ω_o values measured in Shanghai and Guangzhou (0.81–0.82) (Yan et al., 2008) but lower than the 0.85–0.9 measured in rural China, 0.85–0.95 in the Northern hemisphere (obtained by AERONET) and 0.92 in a Hong Kong rural area during the winter period (Table 3).

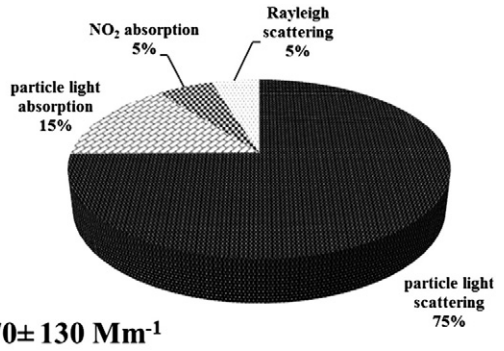

Fig. 3. Optical contribution to total light extinction (B_{ext}) based on hourly averaged dry particle light scattering (B_{sp}), particle light absorption (B_{ap}), NO_2 absorption and Rayleigh scattering.

In general, light extinction (B_{ext}) includes particle light scattering (B_{sp}), particle absorption (B_{ap}), gaseous light scattering (B_{sg}) and gaseous light absorption (B_{ag}) (Bohren and Huffman, 2008). Light scattering from gaseous matter is defined as Rayleigh scattering, which is defined by US IMPROVE as 13 Mm^{-1}. But gaseous light absorption is mainly from NO_2 (Horvath, 1993; Bohren and Huffman, 2008), which can be calculated from the NO_2 concentration (ppb) multiplied by 0.33 (Pitchford et al., 2007). As shown in Fig. 3, the particulate matter B_{sp} is the highest contributor, accounting for ~75% of total light extinction (B_{ext}). The B_{ap} contributed 15% of the B_{ext}, while the remaining 10% was attributed to gaseous (NO_2) absorption and Rayleigh scattering.

Table 3
Examples of particle scattering (B_{sp}), absorption (B_{ap}) and SSA (ω_o) measured from past studies.

Site (urban site)	Period (month, year)	B_{sp} (Mm^{-1})	B_{ap} (Mm^{-1})	SSA ω_o	Instrumentation	References
HKPU, HK	Oct.–Dec., 2010	202	40	0.82	● M9003 Nephelometer EcoTech ● AE-31, Magee scientific	This study
Beijing, China	Winter, 2004	259	58	0.82	● Nephelometer, Radiance research PASP, Radiance Research, M903	(He et al., 2009)
Guangzhou, China	Oct.–Nov., 2004	418	91	0.80	● Nephelometer, Radiance Research, ● M903 PAS	(Andreae et al., 2008)
Shanghai, China	Dec., 2010–Mar., 2011	293	66	0.81	● M9003 Nephelometer, Eco Tech ● AE-31 Magee Scientific,	(Xu et al., 2012)
Valencia, Spain	Winter, 2006–2010(average)	60	N.A.	N.A.	● 3563 Nephelometer, TSI, Inc.	(Esteve et al., 2012)
Granada, Spain	Winter, 2005	84	28	0.75	● 3563 Nephelometer, TSI, Inc. ● 5012 MAAP, Thermo, Inc.	(Lyamani et al., 2008)
Southern Mexico City	Feb. 2005	93	20	0.82	● Nephelometer, Radiance research ● PASP, RadianceResearch, M903	(Garcia et al., 2010)

N.A. = not available.

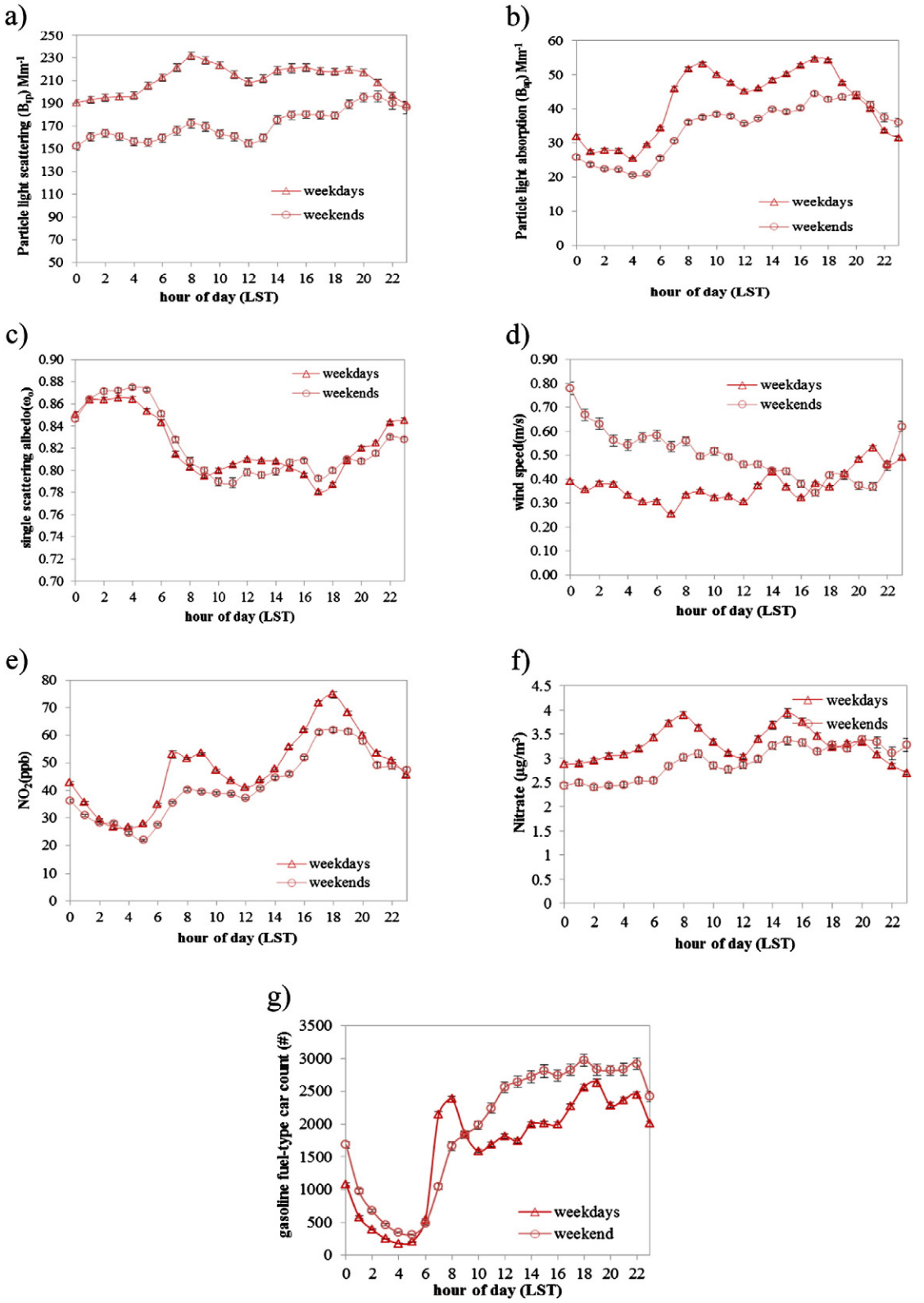

Fig. 4. Diurnal variation of: a) hourly dry particle light scattering coefficient (B_{sp}); b) hourly particle absorption coefficient (B_{ap}); c) single scattering albedo (ω_o); d) wind speeds; e) NO_2; f) nitrate; and g) gasoline-typed vehicle counts (#).

3.2. Temporal variation of aerosol optical properties

The value of the optical components was averaged for each hour of the day during the October to December 2010 period, to obtain the average measurements as a function of local standard time (LST). The B_{sp} and B_{ap} showed clear diurnal variation with small standard errors (Fig. 4). Their respective values were found to be 22% and 24% higher on weekdays than on weekends. A similar morning peak in B_{sp} was observed around 08:00 LST on weekdays and weekends (Fig. 4a). A slight increase in B_{sp} in the afternoon (14:00–16:00 LST) is related to secondary aerosol formation by the photochemical reaction of gaseous precursors (Yan et al., 2008). But a sharp increase was only found during the late afternoon period (18:00–20:00 LST) on weekends, with weekdays instead showing a decrease over this period. In addition, similar patterns were observed over this period in NO_3^- (Fig. 4f) and vehicle count (Fig. 4g), which could reflect the increase in local traffic activity. For the particle light absorption (B_{ap}), an elevated value (53–54 Mm^{-1}) occurred during the morning (8:00–9:00 LST) and afternoon (17:00–18:00 LST) rush hours on weekdays (Fig. 4b). Weekends exhibited more prolonged morning (8:00–11:00 LST) and afternoon (17:00–20:00 LST) peaks with lower values of 37.4 Mm^{-1} and 44.4 Mm^{-1}, respectively. The decrease of B_{ap} at noon (12:00 LST) suggests that the increase in the planetary boundary layer (PBL) and higher wind speeds cause more efficient dispersion (Fig. 4d). Lower B_{ap} values in the early morning were observed, potentially due to dry deposition causing particle removal. Previous studies (Titos et al., 2012; Xu et al., 2012; Yan et al., 2008) have shown that BC, as a primary pollutant, is the main contributor to B_{ap}, and similar diurnal pattern of B_{ap} has been found at urban sites in Spain and Shanghai and a Beijing rural site. The evening peak (20:00–21:00 LST) found during the weekend coincides with the increase in hourly-averaged NO_2 (Fig. 4e), NO_3^- (Fig. 4f) and traffic counts (Fig. 4g) (Hong Kong Transportation Department). For this reason, the diurnal variation of single scattering albedo (SSA, ω_o; Fig. 4c) showed a maximum value during the early morning hours (02:00–04:00 LST) and decreased to a minimum in the early traffic hours and late afternoon. The diurnal pattern of single scattering albedo indicated a reduction of light absorption loading in the early morning due to dry deposition particle removal.

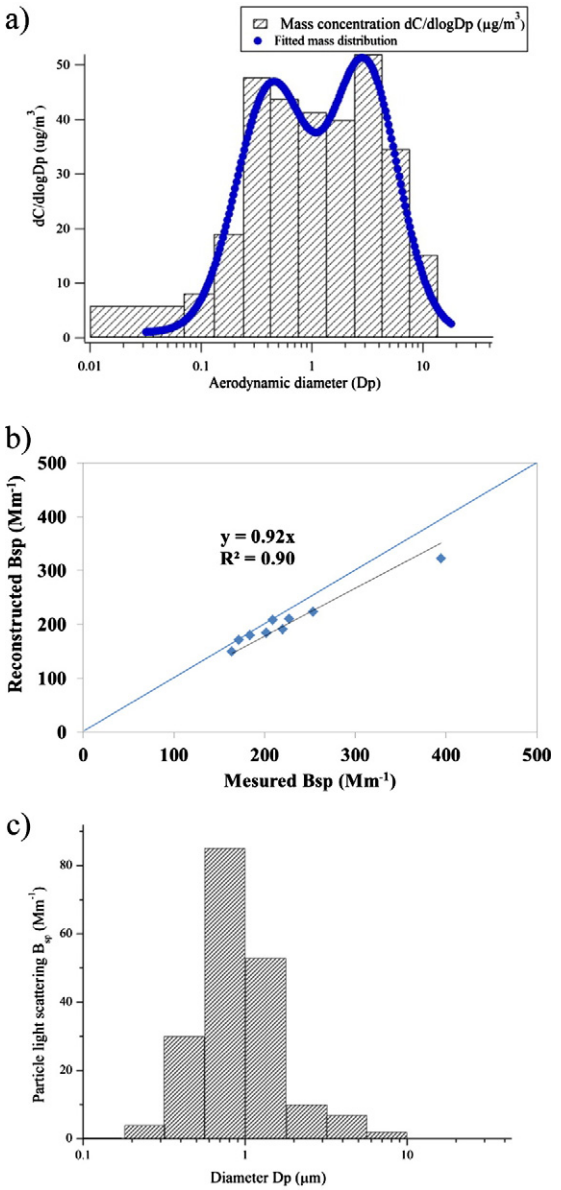

Fig. 5. a) Size distribution on particle mass concentration. b) Relationship of reconstructed B_{sp} and measured B_{sp}. c) Size distribution on aerosol B_{sp} (averaged over 9 days).

3.3. Chemical and optical characteristics of size-resolved particles

The particle size modes were defined as follows: a coarse mode (1.8–10 μm), droplet mode (0.56–1.8 μm), condensation mode (0.1–0.56 μm) and nucleation mode (<0.1 μm). Particle light scattering and absorption varied with particle size (Chow et al., 2002; Kleefeld et al., 2002; Watson, 2002; Yu et al., 2010). Fig. 5a shows a bimodal size distribution, which dominated in coarse mode with a mass median aerodynamic diameter

Table 4
Measured (optical) and size-resolved (chemical) reconstructed particle light scattering coefficient.

Sampling date (2010)	Measured particle light scattering (Mm^{-1})[a]	Reconstructed PM_{10} light scattering (Mm^{-1})[b] 0–10 μm	Reconstructed $PM_{1.8}$ light scattering (Mm^{-1})[b] 0–1.8 μm
Oct. 23–24	171.7	196.3	184.0
Nov. 1–2	253.4	282.4	265.1
Nov. 4–5	394.4	418.4	407.3
Nov. 7–8	202.2	237.3	229.9
Nov. 13–14	163.8	222.6	191.5
Nov. 25–26	219.8	247.9	234.0
Dec. 1–2	227.4	272.1	260.5
Dec. 5–6	253.3	287.4	263.6
Dec. 11–12	210.2	203.7	191.5
Average	232.9	263.1	247.5

[a] Measured by Nephelometer at λ of 532 nm.
[b] Calculation based on Eq. (2).

Table 5
Contribution to particle light extinction (B_{ext}) for different size-resolved chemical species.[a].

PU	Total mass	Ammonium sulfate	Ammonium nitrate	Organic matters	Elemental carbon	Soil dust	Sea salt
Coarse mode (1.8–10 μm)	4%	1%	Nil [c]	1%	<1%	1%	<1%
Droplet mode (0.56–1.8 μm)	74%	20%	4%	43%	2%	5%	<1%
Condensation mode (0.1–0.56 μm)	22%	7%	1.1%	8%	5%	1%	<1%
Nucleation mode (<0.1 μm)	0.4%	N.A[b].	N.A.[b]	N.A.[b]	0.4%	N.A[b].	N.A[b].

[a] The particle B_{ext} data calculated based on the Eq. (4).
[b] The data is below 0.1%.
[c] The data is not available.

(MMAD, D_{pg1}) of 3 μm and a standard deviation (σ_{g1}) of 2.87, and condensation mode, with an MMAD (D_{pg2}) of 0.4 μm and a standard deviation (σ_{g2}) of 2.98. The mass concentration for each mode constituted ~26% of the total PM_{18} mass.

The US IMPROVE equation is not suitable for determining the optical properties of size-resolved particles. For this reason, Mie theory was also used in this study. Fig. 5b shows a good correlation ($R^2 = 0.9$) between the nephelometer-measured and chemical-reconstructed fine particle B_{sp}, with a regression slope of ~0.92 based on Eq. (2) and the sum of MOUDI stages excluding EC, NO_2 and Rayleigh scattering.

Fig. 5c show the single mode particle B_{sp} distribution with a peak in the droplet mode (0.56–1.8 μm). Coarse particles accounted for only ~5% of the particle B_{sp}. The average PM_{10} light scattering was primarily due to fine particles, $PM_{1.8}$ (~94%) (Table 4). This is consistent with the results of previous studies (Deng et al., 2008), indicating that fine particles are the main contributor to visibility impairment. As shown in Table 5, the droplet mode accounted for 74% of the total particle B_{ext}, further confirming the importance of small particles (0.56–1.0 μm) in visibility degradation (Table 5).

To better understand their chemical and optical characteristics, particles have been divided into four size groups, the nucleation mode (<0.1 μm), condensation mode (0.1–0.56 μm), droplet mode (0.56–1.8 μm) and coarse mode (1.8–10 μm). Table 5 shows that soil dust contributes the most in the coarse mode and that contributions from EC are low and predominately in the condensation mode. Organic matter was the largest contributor to B_{ext} in the droplet mode (~43%) and condensation mode (~8%), suggesting the influence of nearby vehicle exhaust. Ammonium sulphate was the second largest contributor, at around 20% in droplet mode, but different result have been found in other urban area studies (Cao et al., 2012; Cheung et al., 2005; Jung et al., 2009; Tao et al., 2009; Wang et al., 2013a). Ammonium nitrate was the largest contributor to visibility impairment in Xi'an (~23%) and Guangzhou (~16%) (Cao et al., 2012; Tao et al., 2009). However, only 4% of B_{ext} in droplet mode and 1% in condensation mode was attributed to this component in this study.

3.4. Source light extinction apportionment

Eighty-one samples (9 stages × 9 samples) were used to identify potential sources and quantify particle source contributions to light extinction in the PMF model using methods similar to Huang et al. (2006) and Cao et al. (2012). A total of 20 base runs and five factors were identified (Fig. 6). The five factors, which were selected based on previous studies in HKPU roadside areas (Cheng, 2007), were soil/fugitive dust, secondary aerosols, sea salt, tire dust, and traffic/vehicle engine exhaust. Detailed source profiles are shown in Figure S4. Factor 1 was identified as soil/fugitive dust (Cheng, 2007), which was dominated by chemical components, Mn, Al, Si, Ca, Ti and Fe. Because there were construction areas around the sampling site, the soil/fugitive dust contribution to particle light extinction was 10%. Factor 2 was the second largest contributor to

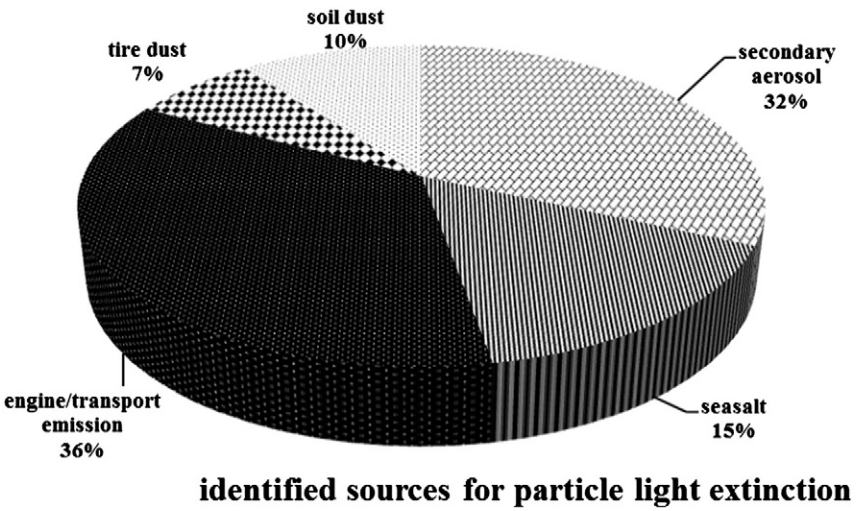

Fig. 6. Percentages of identified sources for particle light extinction (B_{ext}).

B_{ext} (~32%) and was abundant in NH_4^+, SO_4^{2-}, NO_3^+ and OC (Huang et al., 2006a), identifying it as the secondary aerosol component. The prevailing northerly wind in the cold season is likely to enhance the transport of these secondary aerosol pollutants. Factor 3 was enriched in Na, Cl^- and nitrate, and was identified as sea salt (Huang et al., 2006). It accounted for ~15% of the total B_{ext}. Factor 4 was identified as tire dust (Cheng, 2007), being dominated by Zn, Mn and Pb. The contribution of tire dust was ~7% of the $B_{ext,}$ due to high traffic volumes close to the sampling site. Factor 5 was dominated by EC and OC and identified as the traffic or vehicle engine exhaust (Cao et al., 2012; Huang et al., 2006). This is the largest contributor to the B_{ext}, accounting for 36% of the total. This large contribution was due to the busy traffic flow near the site at the Cross Harbour Tunnel. Therefore, the local visibility impairment was primarily due to the traffic emissions and the regional secondary aerosol pollution.

4. Conclusion

Hourly particle light scattering and absorption coefficients, gaseous NO_2, meteorological parameters (i.e. RH, wind speed, temperature) and 24-h size-resolved particle measurements were collected in a Hong Kong urban area from October 23rd to December 31st, 2010 to investigate the temporal variability of optical properties and the contributing chemical components. The average particle light scattering (B_{sp}) and absorption coefficients (B_{ap}) were 201.96 ± 105.82 Mm^{-1} and 39.91 ± 19.16 Mm^{-1}, respectively. The majority of particle light extinction (B_{ext}) was due to particle scattering, with an SSA (ω_o) of 0.82 ± 0.07. The diurnal variation pattern for particle B_{sp} differed between weekdays and weekends, when elevated particle B_{sp} values were found during the late evening hours.

Based on Eq. (2), it is clear that particle size rather than mass most directly affects particle B_{ext}. Droplet mode (0.56–1.8 μm) particles contributed the most to particle B_{ext}, compared to other four size groups. Within this mode, organic matter had the highest contribution (~41%) to particle B_{ext}. Organic matter and ammonium sulphate were the highest contributors to the condensation mode (0.1–0.56 μm), accounting for ~8% and 7% of B_{ext}, respectively, followed by elemental carbon (~5%).

By using the PMF model, five source factors were determined. Traffic/engine exhaust was the largest source, accounting for ~36% of B_{ext}, followed by secondary aerosols (~32%), sea salt (~15%), soil dust (~10%) and tire dust (~7%).

Acknowledgements

The authors would like to acknowledge the financial support of the Environmental Conservation Fund of Hong Kong (7/2009), the National Natural Science Foundation of China (41105083 and 41275130) and the Guangdong Natural Science Foundation (S2012010009824 and S2011040005259).

Appendix A. Supplementary data

Supplementary data to this article can be found online at http://dx.doi.org/10.1016/j.atmosres.2014.10.020.

References

Andreae, M.O., Schmid, O., Yang, H., Chand, D., Yu, J.Z., Zeng, L.M., Zhang, Y.H., 2008. Optical properties and chemical composition of the atmospheric aerosol in urban Guangzhou, China. Atmos. Environ. 42, 6335–6350.
Ångström, A., 1930. On the atmospheric transmission of sun radiation. II. Geogr. Ann. 130–159.
Aurora-1000 Single Wavelength Integrating Nephelometer User Manual, 2008. Ecotech Environmental Monitoring., Australia.
Bergin, M.H., Ogren, J.A., Schwartz, S.E., McInnes, L.M., 1997. Evaporation of ammonium nitrate aerosol in a heated nephelometer: implications for field measurements. Environ. Sci. Technol. 31, 2878–2883.
Bohren, C.F., Huffman, D.R., 2008. Absorption and Scattering of Light by Small Particles. Wiley.com.
Cao, J.J., Wang, Q.Y., Chow, J.C., Watson, J.G., Tie, X.X., Shen, Z.X., Wang, P., An, Z.S., 2012. Impacts of aerosol compositions on visibility impairment in Xi'an, China. Atmos. Environ. 59, 559–566.
Chang, W.L., Koo, E.H., 1986. A study of visibility trends in Hong Kong (1968–1982). Atmos. Environ. 20, 1847–1858.
Cheng, Y., 2007. The Characteristics and Source Identification of Airborne Particles at the Roadside of Hong Kong-PolyU (PU) Supersite.
Cheng, Y.F., Wiedensohler, A., Eichler, H., Su, H., Gnauk, T., Brüggemann, E., Herrmann, H., Heintzenberg, J., Slanina, J., Tuch, T., Hu, M., Zhang, Y.H., 2008. Aerosol optical properties and related chemical apportionment at Xinken in Pearl River Delta of China. Atmos. Environ. 42, 6351–6372.
Cheung, H.-C., Wang, T., Baumann, K., Guo, H., 2005. Influence of regional pollution outflow on the concentrations of fine particulate matter and visibility in the coastal area of southern China. Atmos. Environ. 39, 6463–6474.
Chow, J.C., Watson, J.G., 1999. Ion chromatography in elemental analysis of airborne particles. Elem. Anal. Airborne Part. 1, 97–137.
Chow, J.C., Watson, J.G., Lowenthal, D.H., Richards, L.W., 2002. Comparability between PM2.5 and particle light scattering measurements. Environ. Monit. Assess. 79, 29–45.
Chow, J.C., Watson, J.G., Lowenthal, D.H., Magliano, K.L., 2005. Loss of PM2.5 nitrate from filter samples in central California. J. Air Waste Manage. Assoc. 55, 1158–1168.
Chow, J.C., Watson, J.G., Chen, L.-W.A., Chang, M.O., Robinson, N.F., Trimble, D., Kohl, S., 2007. The IMPROVE_A temperature protocol for thermal/optical carbon analysis: maintaining consistency with a long-term database. J. Air Waste Manage. Assoc. 57, 1014–1023.
Chow, J.C., Watson, J.G., Lowenthal, D.H., Antony Chen, L.W., Motallebi, N., 2011. PM2.5 source profiles for black and organic carbon emission inventories. Atmos. Environ. 45, 5407–5414.
Clegg, S.L., Seinfeld, J.H., 2004. Improvement of the Zdanovskii–Stokes–Robinson Model for Mixtures Containing Solutes of Different Charge Types. J. Phys. Chem. A 108, 1008–1017.
Clegg, S.L., Brimblecombe, P., Wexler, A.S., 1998. Thermodynamic model of the system H + −NH4 + −SO42−−NO3−−H2O at tropospheric temperatures. J. Phys. Chem. A 102, 2137–2154.
Deng, X.J., Tie, X.X., Wu, D., Zhou, X.J., Bi, X.Y., Tan, H.B., Li, F., Hang, C.L., 2008. Long-term trend of visibility and its characterizations in the Pearl River Delta (PRD) region, China. Atmos. Environ. 42, 1424–1435.
Dong, Y., Hays, M.D., Dean Smith, N., Kinsey, J.S., 2004. Inverting cascade impactor data for size-resolved characterization of fine particulate source emissions. J. Aerosol Sci. 35, 1497–1512.
Esteve, A.R., Estellés, V., Utrillas, M.P., Martínez-Lozano, J.A., 2012. In-situ integrating nephelometer measurements of the scattering properties of atmospheric aerosols at an urban coastal site in western Mediterranean. Atmos. Environ. 47, 43–50.
Garcia, L.Q., Castro, T., Saavedra, M.I., Martinez-Arroyo, M.A., 2010. Optical properties of aerosols: southern Mexico City. Atmosfera 23, 403–408.
Han, J., Moon, K., Lee, S., Kim, Y., Ryu, S., Cliff, S., Yi, S., 2006. Size-resolved source apportionment of ambient particles by positive matrix factorization at Gosan background site in East Asia. Atmos. Chem. Phys. 6, 211–223.
Hand, J.L., Malm, W.C., 2007. Review of aerosol mass scattering efficiencies from ground-based measurements since 1990. J. Geophys. Res.-Atmos. 112, D16203.
He, X., Li, C.C., Lau, A.K.H., Deng, Z.Z., Mao, J.T., Wang, M.H., Liu, X.Y., 2009. An intensive study of aerosol optical properties in Beijing urban area. Atmos. Chem. Phys. 9, 8903–8915.
Ho, K., Lee, S., Yu, J.C., Zou, S., Fung, K., 2002. Carbonaceous characteristics of atmospheric particulate matter in Hong Kong. Sci. Total Environ. 300, 59–67.
Ho, K.F., Lee, S.C., Cao, J.J., Chow, J.C., Watson, J.G., Chan, C.K., 2006. Seasonal variations and mass closure analysis of particulate matter in Hong Kong. Sci. Total Environ. 355, 276–287.

Horvath, H., 1993. Atmospheric light absorption—a review. Atmos. Environ. Part A Gen. Topic 27, 293–317.
Hong Kong Observatory (HKO), 2013. Long term trend of the annual number of hours of reduction visibility in Hong Kong from 1968 to 2013. , http://www.hko.gov.hk/cis/statistic/hko_redvis_statistic_e.htm.
Huang, Z., Harrison, R.M., Allen, A.G., James, J.D., Tilling, R.M., Yin, J., 2004. Field intercomparison of filter pack and impactor sampling for aerosol nitrate, ammonium, and sulphate at coastal and inland sites. Atmos. Res. 71, 215–232.
Huang, X.F., Yu, J.Z., He, L.Y., Hu, M., 2006. Size distribution characteristics of elemental carbon emitted from Chinese vehicles: results of a tunnel study and atmospheric implications. Environ. Sci. Technol. 40, 5355–5360.
Jung, J., Lee, H., Kim, Y.J., Liu, X., Zhang, Y., Gu, J., Fan, S., 2009. Aerosol chemistry and the effect of aerosol water content on visibility impairment and radiative forcing in Guangzhou during the 2006 Pearl River Delta campaign. J. Environ. Manag. 90, 3231–3244.
Kleefeld, C., O'Dowd, C.D., O'Reilly, S., Jennings, S.G., Aalto, P., Becker, E., Kunz, G., de Leeuw, G., 2002. Relative contribution of submicron and supermicron particles to aerosol light scattering in the marine boundary layer. J. Geophys. Res.-Atmos. 107.
Lai, L.Y., Sequeira, R., 2001. Visibility degradation across Hong Kong: its components and their relative contributions. Atmos. Environ. 35, 5861–5872.
Lee, Y.L., Sequeira, R., 2002. Water-soluble aerosol and visibility degradation in Hong Kong during autumn and early winter, 1998. Environ. Pollut. 116, 225–233.
Li, X., He, K., Li, C., Yang, F., Zhao, Q., Ma, Y., Cheng, Y., Ouyang, W., Chen, G., 2013. PM2.5 mass, chemical composition and light extinction before and during the 2008 Beijing Olympics. J. Geophys. Res. : Atmos JD020106.
Ling, Z.H., Guo, H., Zheng, J.Y., Louie, P.K.K., Cheng, H.R., Jiang, F., Cheung, K., Wong, L.C., Feng, X.Q., 2013. Establishing a conceptual model for photochemical ozone pollution in subtropical Hong Kong. Atmos. Environ. 76, 208–220.
Lowenthal, D.H., Kumar, N., 2004. Variation of mass scattering efficiencies in IMPROVE. J. Air Waste Manage. Assoc. 54, 926–934.
Lowenthal, D., Kumar, N., 2006. Light scattering from sea-salt aerosols at Interagency Monitoring of Protected Visual Environments (IMPROVE) sites. J. Air Waste Manage. Assoc. 56, 636–642.
Lowenthal, D.H., Rogers, C.F., Saxena, P., Watson, J.G., Chow, J.C., 1995. Sensitivity of estimated light extinction coefficients to model assumptions and measurement errors. Atmos. Env. 29, 751–766.
Lyamani, H., Olmo, F.J., Alados-Arboledas, L., 2008. Light scattering and absorption properties of aerosol particles in the urban environment of Granada, Spain. Atmos. Environ. 42, 2630–2642.
Malm, W.C., Pitchford, M.L., 1997. Comparison of calculated sulfate scattering efficiencies as estimated from size-resolved particle measurements at three national locations. Atmos. Environ. 31, 1315–1325.
Malm, W.C., Sisler, J.F., Huffman, D., Eldred, R.A., Cahill, T.A., 1994. Spatial and seasonal trends in particle concentration and optical extinction in the United States. J. Geophys. Res. 99, 1347–1370.
Man, C.K., Shih, M.Y., 2001. Light scattering and absorption properties of aerosol particles in Hong Kong. J. Aerosol Sci. 32, 795–804.
Mie, G., 1908. Beiträge zur Optik trüber Medien, speziell kolloidaler Metallösungen. Ann. Phys. 330, 377–445.
Milford, J.B., Davidson, C.I., 1987. The sizes of particulate sulfate and nitrate 1B the atmosphere—a-review. JAPCA 37, 125–134.
Nie, W., Wang, T., Gao, X., Pathak, R.K., Wang, X., Gao, R., Zhang, Q., Yang, L., Wang, W., 2010. Comparison among filter-based, impactor-based and continuous techniques for measuring atmospheric fine sulfate and nitrate. Atmos. Environ. 44, 4396–4403.
Paatero, P., 1997. Least squares formulation of robust non-negative factor analysis. Chemom. Intell. Lab. Syst. 37, 23–35.
Paatero, P., Tapper, U., 1994. Positive matrix factorization: a non-negative factor model with optimal utilization of error estimates of data values. Environmetrics 5, 111–126.
Pitchford, M., Malm, W., Schichtel, B., Kumar, N., Lowenthal, D., Hand, J., 2007. Revised algorithm for estimating light extinction from IMPROVE particle speciation data. J. Air Waste Manage. Assoc. 57, 1326–1336.
Rocard, Y., de Rothschild, P., 1927. Diffusion de la lumiere et visibilite. Rev. Opt. 6, 353.
Rosenberg, P.D., Dean, A.R., Williams, P.I., Dorsey, J.R., Minikin, A., Pickering, M.A., Petzold, A., 2012. Particle sizing calibration with refractive index correction for light scattering optical particle counters and impacts upon PCASP and CDP data collected during the Fennec campaign. Atmos. Meas. Technol. 5, 1147–1163.
Rosenfeld, D., 1999. TRMM observed first direct evidence of smoke from forest fires inhibiting rainfall. Geophys. Res. Lett. 26, 3105–3108.
Sequeira, R., Lai, K.-H., 1998. The effect of meteorological parameters and aerosol constituents on visibility in urban Hong Kong. Atmos. Environ. 32, 2865–2871.
Sisler, J.F., Malm, W., Gebhart, K., Pitchford, M.L., 1996. Spatial and seasonal patterns and long term variability of the composition of the haze in the United States. Report ISSN, pp. 0737–5352.
Sloane, C.S., 1983. Optical properties of aerosols—Comparison of measurements with model calculations. Atmos. Environ. 17, 409–416.
Sloane, C.S., 1984. Optical properties of aerosols of mixed composition. Atmos. Environ. 18, 871–878.
Sloane, C.S., 1986. Effect of composition on aerosol light scattering efficiencies. Atmos. Environ. 20, 1025–1037.
Sloane, C.S., Wolff, G.T., 1985. Prediction of ambient light scattering using a physical model responsive to relative humidity: validation with measurements from Detroit. Atmos. Environ. 19, 669–680.
Stokes, R.H., Robinson, R.A., 1966. Interactions in aqueous nonelectrolyte solutions. I. Solute–solvent equilibria. J. Phys. Chem. 70, 2126–2131.
Tang, I.N., 1996. Chemical and size effects of hygroscopic aerosols on light scattering coefficients. J. Geophys. Res.-Atmos. 101, 19245–19250.
Tao, J., Ho, K.-F., Chen, L., Zhu, L., Han, J., Xu, Z., 2009. Effect of chemical composition of $PM_{2.5}$ on visibility in Guangzhou, China, 2007 spring. Particuology 7, 68–75.
Titos, G., Foyo-Moreno, I., Lyamani, H., Querol, X., Alastuey, A., Alados-Arboledas, L., 2012. Optical properties and chemical composition of aerosol particles at an urban location: an estimation of the aerosol mass scattering and absorption efficiencies. J. Geophys. Res.-Atmos. 117.
Tsai, J.-H., Lin, J.-H., Yao, Y.-C., Chiang, H.-L., 2012. Size distribution and water soluble ions of ambient particulate matter on episode and non-episode days in Southern Taiwan. Aerosol Air Qual. Res. 12, 263–274.
Twomey, S., 1975. Comparison of constrained linear inversion and an iterative nonlinear algorithm applied to the indirect estimation of particle size distributions. J. Comput. Phys. 18, 188–200.
Wang, T., Group,H.K.E.P.D.A.S., Technology, H.K.P.U.R.C.f.E., Management, 2003. Study of Visibility Reduction and Its Causes in Hong Kong: Final Report. Research Centre for Environmental Technology and Management, Department of Civil and Structural Engineering, Hong Kong Polytechnic University.
Wang, Q., Cao, J., Tao, J., Li, N., Su, X., Chen, L.W.A., Wang, P., Shen, Z., Liu, S., Dai, W., 2013a. Long-term trends in visibility and at Chengdu, China. PLoS ONE 8, e68894.
Wang, X., Wang, T., Pathak, R., Hallquist, M., Gao, X., Nie, W., Xue, L., Gao, J., Gao, R., Zhang, Q., Wang, W., Wang, S., Chai, F., Chen, Y., 2013b. Size distributions of aerosol sulfates and nitrates in Beijing during the 2008 Olympic Games: impacts of pollution control measures and regional transport. Adv. Atmos. Sci. 30, 341–353.
Watson, J.G., 2002. Visibility: science and regulation. J. Air Waste Manage. Assoc. 52, 628–713.
Watson, J.G., Chow, J.C., Frazier, C.A., 1999. X-ray fluorescence analysis of ambient air samples, In: Landsberger, S., Creatchman, M., Vo-Dinh, T. (Eds.), Advances in Environmental Industrial and Process Control Technologies: V, 1st ed. Gordon and Breach Science Publishers, Amsterdam, The Netherlands.
Watson, J.G., Antony Chen, L.W., Chow, J.C., Doraiswamy, P., Lowenthal, D.H., 2008a. Source apportionment: findings from the U.S. supersites program. J. Air Waste Manage. Assoc. 58, 265–288.
Watson, J.G., Chow, J.C., Lowenthal, D.H., Magliano, K.L., 2008b. Estimating aerosol light scattering at the Fresno Supersite. Atmos. Environ. 42, 1186–1196.
Weingartner, E., Saathoff, H., Schnaiter, M., Streit, N., Bitnar, B., Baltensperger, U., 2003. Absorption of light by soot particles: determination of the absorption coefficient by means of aethalometers. J. Aerosol Sci. 34, 1445–1463.
Winklmayr, W., Wang, H.-C., John, W., 1990. Adaptation of the Twomey algorithm to the inversion of cascade impactor data. Aerosol Sci. Technol. 13, 322–331.
Wiscombe, W.J., 1980. Improved Mie scattering algorithms. Appl. Opt. 19, 1505–1509.
World Bank, 2011. Annual report. , http://siteresources.worldbank.org/EXTANNREP2011/Resources/8070616-1315496634380/WBAR11_YearInReview.pdf.
Wu, D., Mao, J.T., Deng, X.J., Tie, X.X., Zhang, Y.H., Zeng, L.M., Li, F., Tan, H.B., Bi, X.Y., Huang, X.Y., Chen, J., Deng, T., 2009. Black carbon aerosols and their radiative properties in the Pearl River Delta region. Sci. China Ser. D Earth Sci. 52, 1152–1163.
Xu, J.W., Tao, J., Zhang, R.J., Cheng, T.T., Leng, C.P., Chen, J.M., Huang, G.H., Li, X., Zhu, Z.Q., 2012. Measurements of surface aerosol optical properties in winter of Shanghai. Atmos. Res. 109, 25–35.
Xu, Z., Wang, T., Xue, L.K., Louie, P.K.K., Luk, C.W.Y., Gao, J., Wang, S.L., Chai, F.H., Wang, W.X., 2013. Evaluating the uncertainties of thermal catalytic conversion in measuring atmospheric nitrogen dioxide at four differently polluted sites in China. Atmos. Environ. 76, 221–226.
Yan, P., Tang, J., Huang, J., Mao, J.T., Zhou, X.J., Liu, Q., Wang, Z.F., Zhou, H.G., 2008. The measurement of aerosol optical properties at a rural site in Northern China. Atmos. Chem. Phys. 8, 2229–2242.

Yu, H., Wu, C., Wu, D., Yu, J.Z., 2010. Size distributions of elemental carbon and its contribution to light extinction in urban and rural locations in the pearl river delta region, China. Atmos. Chem. Phys. 10, 5107–5119.

Zhou, Y., Wang, T., Gao, X., Xue, L., Wang, X., Wang, Z., Gao, J., Zhang, Q., Wang, W., 2009. Continuous observations of water-soluble ions in PM2. 5 at Mount Tai (1534 m asl) in central-eastern China. J. Atmos. Chem. 64, 107–127.

Zhou, S., Wang, Z., Gao, R., Xue, L., Yuan, C., Wang, T., Gao, X., Wang, X., Nie, W., Xu, Z., Zhang, Q., Wang, W., 2012. Formation of secondary organic carbon and long-range transport of carbonaceous aerosols at Mount Heng in South China. Atmos. Environ. 63, 203–212.